Short Communication

Corrosion Resistance of Electroplating of Cu–Ni/P Coatings on NdFeB Magnet Materials

Fan Wang[1], Xiao Ping Chen[2], Ping Qiu[3], Xiang Dong Wang[2], Wei Lu [1]

[1] Shanxi Special Equipment Inspection and Testing Institute,Xi'an 710048,China
[2] Division of Engineering Steeel, Cenlral Iron and Steel Research Institute, Beijing 100081, China
[3] China University of Petroleum-Beijing, Beijing 102249, China
[*]E-mail: wangfan_0109@163.com

The aim of this study is to improve the NdFeB (Ni–Cu–Ni) plating process by reducing the magnetic shielding effect for the underlying Ni of the substrate and improving corrosion resistance. Two kinds of copper and Ni/P composite coatings on NdFeB magnets were successfully prepared with plating technology. Coating surface and cross-sectional morphologies were observed by scanning electron microscopy. Chemical composition of the coatings was studied through energy-dispersive spectroscopy, X-ray diffraction, and X-ray photoelectron spectroscopy. Corrosion resistances of the copper coating and Ni/P coatings were evaluated by potentiodynamic polarization and electrochemical tests, respectively. In the salt spray test, coatings exhibited good corrosion resistance ability. Results of the corrosion test in 3.5 wt.% sodium chloride solution, showed that the Cu–Ni/P composite coating provided excellent anti-corrosion performance for the magnets.

1. INTRODUCTION

NdFeB permanent magnets have excellent magnetic properties. However, owing to the presence of the Nd-rich phase [1–4], NdFeB magnets are highly affected by corrosion in humid environments Corrosion causes significant magnetic deterioration [5]. In a humid environment, the hydrogen absorption process of the magnet is as follows: first the neodymium-rich phase structure exposed on the surface adsorbs hydrogen, followed by the reaction of the main phase $Nd_2Fe_{14}B$ with hydrogen, and then there is the reaction of the neodymium-rich phase to generate $Nd(OH)_3$. Hydrogen gas will also be generated, and the hydrogen absorption reaction will be repeatedly triggered. In acidic media, the neodymium and iron of the magnet material cause the reaction of hydrogen ions in the medium to generate hydrogen gas, which will also cause hydrogen absorption powdering of the

permanent magnetic material. Currently, adding a small amount of alloying elements or by coating the surface of the NdFeB permanent magnet with metal or organic coatings with good corrosion resistance is used to increase the corrosion resistance of the magnetic material [5–11].To improve the corrosion resistance of NdFeB, the electrodeposition technique, which is proper surface protection treatment of the magnet can greatly improve the corrosion resistance of the magnet without affecting the magnetic characteristics of the NdFeB magnet itself, and the cost can also be controlled to a certain extent. In addition, this method also has certain technical controllability [2,12–16].

Duing to its simplicity and effectiveness, the coating material plays an important role in the electrodeposition of the magnet. Common coating materials include: (i) surface plating nickel, zinc, or aluminum plating, (ii) Ni/P amorphous coatings, and (iii) Al–Cr, silane, or other chemical conversion coatings [5,17–22]. However, each material has its own limitations. Currently, NdFeB plating is not just a single metal plating but a multilayer metal plating. Recent research has showed that NdFeB magnet materials cannot immediately execute copper coating plating. Traditional plating techniques, such as electroplating Ni coatings, Ni–Cu–Ni plating, and multilayered coatings [23], have been used to protect sintered NdFeB magnets [24]. For the Ni–Cu–Ni multilayer coatings, the innermost Ni coatings have certain magnetic shielding effects on the substrate [25]. Therefore, in this work, to reduce the magnetic shielding effects on the properties of NdFeB, corrosion resistance and the electroplating of Cu–Ni/P multilayer coatings have been studied. Copper coating is generally not used as the protective layer of parts, but it is used as a protective decorative coating of the bottom layer or, most commonly, the middle layer. Copper coating surface coverage is good and activates the surface easily. It is easily covered by other metal coatings and provides good adhesion between the coatings. We used Ni/P composite coatings to replace the outermost Ni coating which is an Ni/P composite coatings. Ni/P composite coatings are widely used in industry to improve the surface properties of various materials due to its good corrosion resistance and excellent wear resistance [26]. In previous research, the microstructures of Ni/P alloys obtained by electroless plating mainly focused on the structural changes from the amorphous phase to the crystalline phase when the phosphorus content was relatively high [27–30]. The phosphorus content in the Ni/P alloy coating is greater than 9 wt.%, has an amorphous structure, and shows better corrosion resistance under deoxidization-acid or chloride environments [31], whereas Ni/P deposits with phosphorus contents less than 5 wt.% have a microcrystalline structure and better corrosion resistance in alkaline media. If the deposits have better resistance against corrosion and abrasion, then phosphorus content should be adjusted and controlled within 10―11 wt.% [31]. Under conditions of equal thickness, higher corrosion resistance of the coating indicates more compact surface passivation film because of the higher phosphorus content of the coating (with or without the heat treatment). In electroplated amorphous Ni/P alloy coatings, there are no grain boundary dislocations such as crystal defects, and intergranular corrosion is not produced. Resistance to pitting corrosion performance is also far better than the crystalline alloy and leads to stress corrosion cracking. Selective corrosion in-sensitive and does not occur during stress corrosion cracking. In addition to excellent corrosion resistance, Ni/P alloy coatings also have high hardness, dense coating, chemical resistance, and good wear resistance, among other characteristics. They are widely used in the chemical, precision machinery, aerospace, and automotive industries.

2. EXPERIMENTAL

2.1. Process

NdFeB magnets were used as substrate materials in this research. Rectangular specimens of 50 mm $\times$ 20 mm $\times$ 30 mm were prepared. The samples were treated as follows: polished $\rightarrow$ degreased with alkaline $\rightarrow$ rinsed with water $\rightarrow$ dipped in 3 vol% nitric acid solution for 30 s $\rightarrow$ ultrasonically cleaned. As shown in Fig. 1, the samples were plated with Cu coating in electroplating solution. The NdFeB magnet samples were used as the cathode, and the copperplate as the anode. The solution contained 5 g/L $Cu_2O_7P_2$, 10 g/L $Na_2B_4O_7 \cdot 10H_2O$, 20 g/L EDTA, and additives. Using $C_3H_6O_3$, the pH value was adjusted to about 7.2. The conditions were as follows: bath temperature was room temperature, deposition time was 1.5 h, and the current density was about 0.2 A/dm^2. After the electroplating copper process, the NdFeB magnets were immersed in a 0.5 vol% sulfuric acid solution for 15 s. Then, the basic plating solution of Ni/P was prepared according to Table 1. Ni/P alloy plating was performed in sulfate baths with the same electrolytic conditions: nickel plate as the anode and NdFeB with copper plating as the cathode. The deposition mechanism of electroplated Ni/P alloy includes a direct deposition mechanism and indirect deposition mechanism. In the direct mechanism: $H_3PO_3 + 3H^+ + 3e^- \rightarrow P + 3H_2O$ (1), $Ni^{2+} + 2e^- \rightarrow Ni$ (2), and $2H^+ + 2e^- \rightarrow H_2$ (3). However, in the indirect reaction mechanism: $6H^+ + 6e^- \rightarrow 6H$ (4), $H_3PO_3 + 6H \rightarrow PH_3 + 3H_2O$ (5), and $2PH_3 + 3Ni_2 + \rightarrow 3Ni + 2P + 6H^+$ (6).
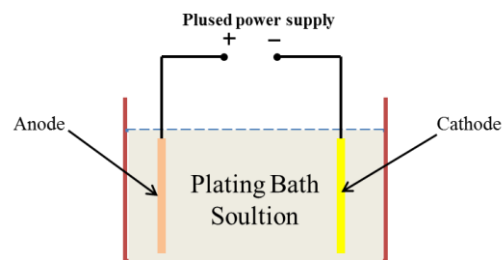
Figure 1. Electroplating device

Table 1. Parameters and solution composition for Ni/P coatings.

Composition	Quantity(g/L)	Parameters
$NiSO_4 \cdot 6H_2O$	200 g/L	Temperature: 50–80 °C
$NiCl_2 \cdot 6H_2O$	20 g/L	Current density: 1–3 A/dm^2
H_3BO_3	20 g/L	Deposition time: 15 min
H_3PO_3	30 g/L	pH: 1–3

2.2. Tests

Ruling experiments (the nick method and SEM) test the binding force between the coating and the substrate.

The surface and sectional morphologies of the copper coating and Ni/P composite coating were characterized using a scanning electron microscope (SEM) (model: S-4300, HITACHI, Japan). The SEM energies used for analysis were 15 kV and 7 μA. The composition of the composite coating was determined using energy-dispersive spectroscopy (EDS) coupled with SEM.

Measurement of potentiodynamic polarization and electrochemical impedance spectroscopy using electrochemical workstation. The measurements were made using a conventional three-electrode battery. The coated specimens were made into working electrodes. Working electrodes were embedded into epoxy resin with an exposure area of 1 cm^2. A platinum sheet and a saturated calomel electrode (SCE) were used as the counter electrode and reference electrode, respectively. Measurements were taken in 3.5 wt% NaCl solution at room temperature. The potential was scanned from −1.0 V to 1.2 V (vs. SCE) with a sweep rate of 0.5 mV/s. The EIS measurement was carried out at room temperature from high frequency to low frequency, i.e., from 10^5 to 10^{-2} Hz.

The salt spray (NSS) test (35 °C, neutral 5.0 wt.% NaCl solutions) was performed using a standard fog chamber in accordance with GB 6461—86 practice (national standard of China for salt spray, which is similar to ASTM G85—98). The angle between the tested sample and the horizontal direction was maintained at 45º, and the settling quantity of salt spray was 1.5 mL/h/80 cm^2 [32]. The spray period for the NSS routine was 24 h.

3. RESULTS AND DISCUSSION

The binding force between the coating and substrate was tested with the nick method. Fig. 2(a) shows the surface of the copper plating layer and composite coatings, which are characterized by cross or parallel lines. The coatings are not peeling or peeling off. Fig. 2(b) shows the close situation between the substrate and coating.
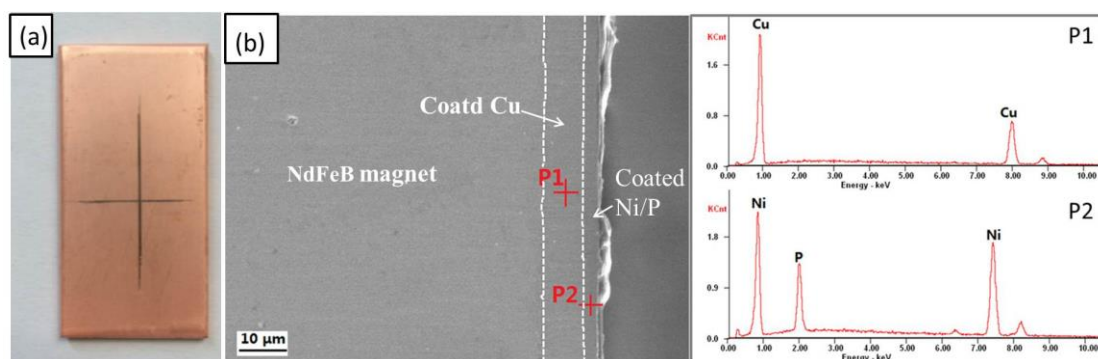
Figure 2. Image of characterization(a) and SEM image of and EDS analyses of the cross section of the Cu–Ni/P-coated NdFeB magnet(b)
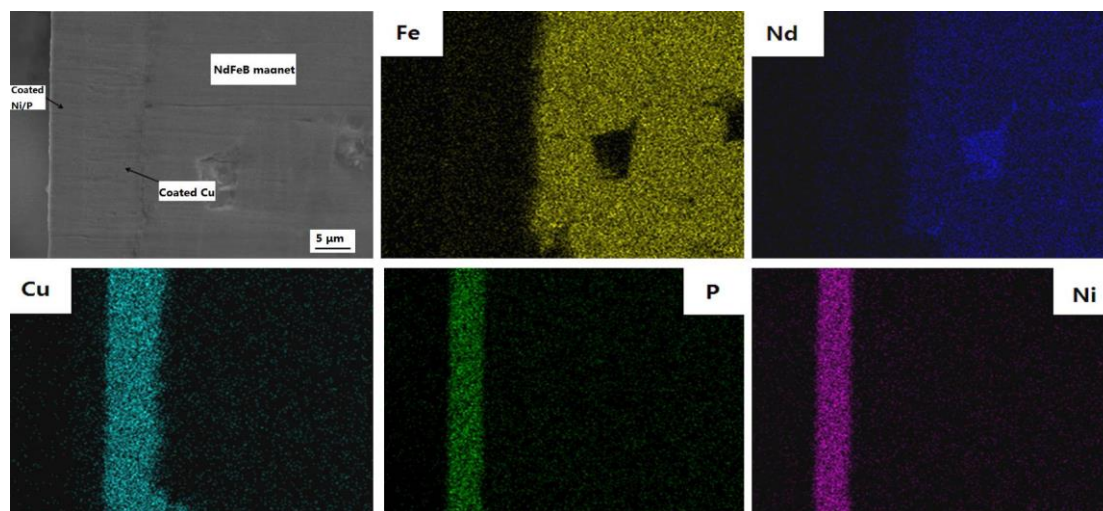
Figure 3. SEM images of the cross section of the Cu–Ni/P-coated NdFeB magnet and EDX mapping of the Cu–Ni/P-coated NdFeB magnet
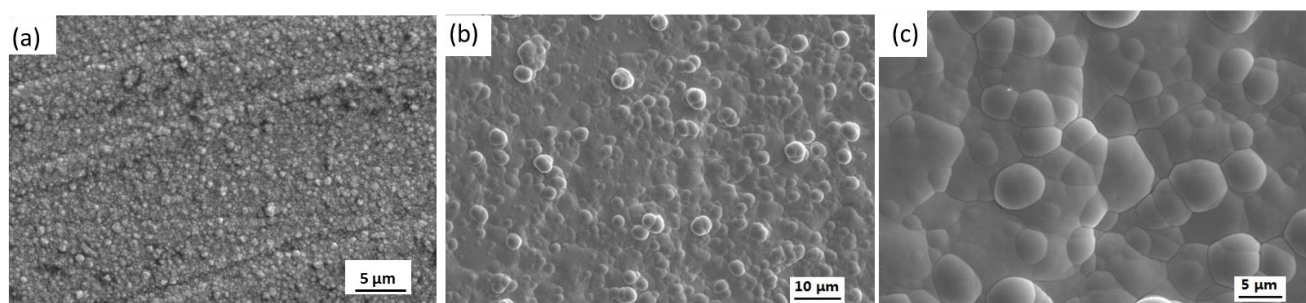
Figure 4. SEM images of the copper coating(a), SEM images of the surface of Ni/P(b) and the enlarged SEM images of the Ni/P coating(c)

The surface microstructures of the coatings were characterized using scanning electron microscope (SEM) and cross-sectional SEM observation. Fig. 3 shows SEM pictures of the cross section of the Cu–Ni/P-coated NdFeB magnet and EDS mapping of the substrate, coated copper, and Ni/P coating. The thickness of the copper coating was about 16 μm. The thickness of the Ni/P coatings was about 10 μm. Fig. 4(a) shows that the copper plating layer covers the substrate very comprehensively, indicating that the copper plating layer protects the substrate very well. The particles of the copper plating layer are basically uniform and dense to provide a good bottom plating layer for the subsequent plating layer. Figs. 4(b) and (c) show SEM images of the surface Ni/P coatings of copper coatings. The Ni/P coating surface exhibits a typical "cauliflower-like" surface, and the shape of the surface is very dense. The size of the "cauliflower-like" cluster is about 13 μm.

Figs. 5(a) and (b) are the XPS spectra of the underlying copper layer. The two peaks of the binding energy are 932.7 eV and 952.5 eV, which correspond to Cu2p3/2 and Cu2p1/2, respectively. The standard Cu2p3/2 peak of elemental copper is located at 932.7 eV. The Cu2p3/2 peaks of Cu (I) and Cu (II) are located at 932.4 eV and 933.8 eV, respectively. It can be concluded from Fig.4(a) that

the copper plating layer does not contain Cu(II). However, elemental copper and Cu(I) Cu2p3/2 are similar, so the Auger peak should be used to determine the state of copper in the coating. Fig. 5 (b) corresponds to Cu LMM, the Auger peak of elemental copper is 918.6 eV, and the standard Auger peak of Cu(I) is 916.8 eV. The Auger peak in Fig. 5(b) proves that there is only elemental copper in the coating. Figs. 5(c) and (d) are the XPS spectra of the Ni/P coating surface. The binding energies of samples Ni2p3/2 are located at 856.8 eV, 853.6 eV, and 852.9 eV. The binding energies of elemental nickel Ni2p1/2 are 870.0 eV and 874.8 eV, indicating that the nickel in the plating layer exists in the zero valence state, and part of the plating layer nickel exists in the form of Ni and P alloys. The peaks of P2p3/2 are at 129.8 eV and 129.6 eV, indicating that the phosphorus and nickel on the surface of the coating form an alloy, and part of the phosphorus P2p and P2p1/2 in the coating exists as a single substance, and their binding energy is between 129.7 eV and 130.3 eV.
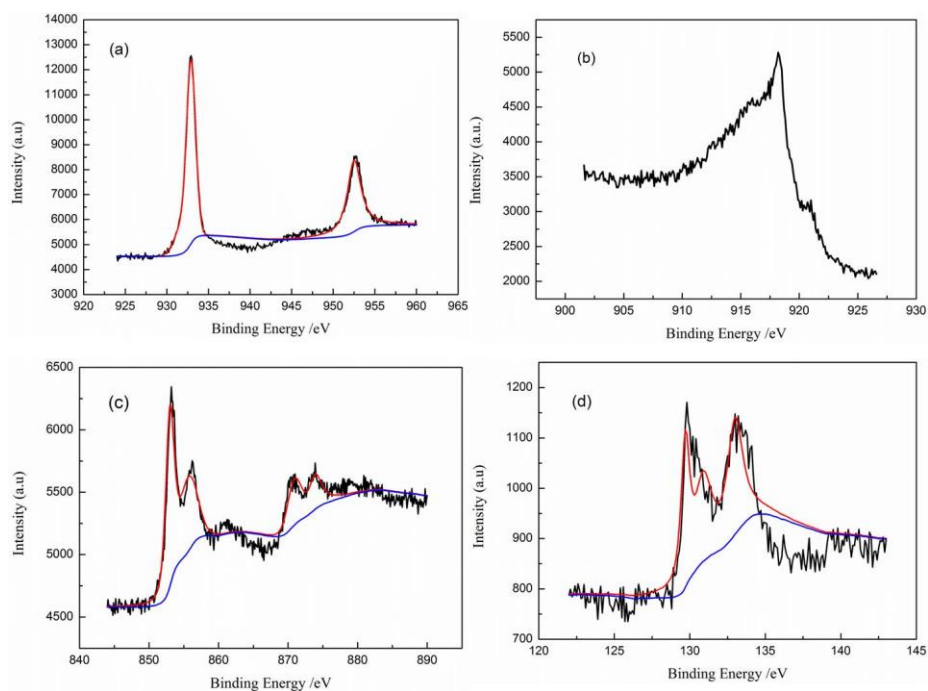
Figure 5. XPS images of coatings

Fig. 6 shows XRD of the surface coatings of pure Ni(a) and Ni/P(b). In Fig. 6(a), the XRD results indicate that the there are sharp diffraction peaks of Ni. They correspond to the three crystal planes of (111), (200), and (220) of Ni, respectively. The radii of Ni and P atoms are 0.125nm and 0.128nm, respectively. Due to the dissolution of P, the nickel lattice is distorted. At this time, P atoms replace the positions of Ni atoms in the Ni lattice, forming Ni as a solvent. With increasing phosphorus content, the crystal lattice is greatly distorted, and the coating is transformed into an amorphous structure. In Fig. 6(b), the surface layer is a nickel-phosphorus alloy-plated coating, which shows the disappearance of diffraction peaks and the appearance of diffuse scattering peaks, which is a process of

gradual distortion of the crystal lattice and the transition to the amorphous state. It can be seen from the figure that the strongest peak appears only at a position with an angle of 2θ of 45°, while the two wings slowly fall within a wide range of diffraction angles and appear to be enveloped, which is a typical amorphous state. It shows that the Ni/P alloy has a typical amorphous structure and no other impure phases appear. It can also be considered that increasing the phosphorus content in the coating to a certain extent causes distortion of the crystal lattice, thereby forming an amorphous structure in which atoms are arranged in a long-range disorder.
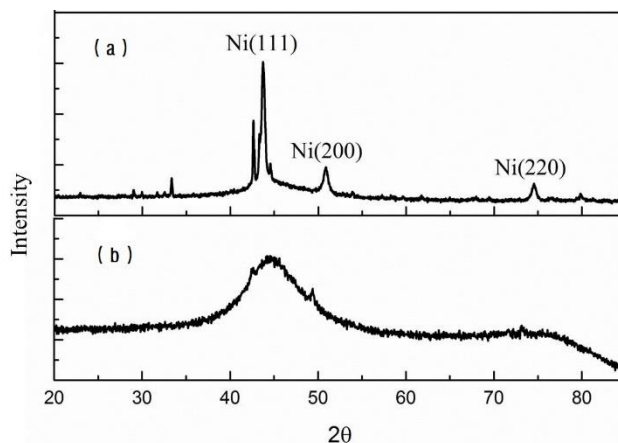
Figure 5. XRD images of surface coatings Ni (a) and Ni/P (b)

The 273A and FRD100 electrochemical workstation was applied to test the potentiodynamic polarization curves of the copper coatings: Ni–Cu–Ni coatings and Cu–Ni/P coatings. 3.5% NaCl aqueous solution was used as the corrosion medium for the electrochemical test, which can determine the possibility of pitting corrosion of coatings in the artificial solution. Chloridion can penetrate through the porosity of coatings and cause pitting corrosion [33].

Fig.7 shows the potentiodynamic polarization curves for coatings on NdFeB. The electrochemical corrosion data could be obtained based on the potentiodynamic polarization curves [33], which are shown in Table 2. For the copper coating, its corrosion potential (E_{corr}) is −676 mV, which is higher than that of the NdFeB substrate. The conventional Ni–Cu–Ni coatings have a corrosion potential of −532 mV. With the increase of polarization potential, the polarization curve of Ni–Cu–Ni coatings turns to a turning point, and the current increases rapidly near the turning point because of the local corrosion of Ni–Cu–Ni coatings. For the Cu–Ni/P composite coatings, its corrosion potential is −515 mV, and the corrosion current density (I_{corr}) after plating is much lower than that of the substrate. The positions of the Cu–Ni/P composite coatings potential polarization curves suggest that Ni/P alloys decrease the corrosion current density of NdFeB. This reduction indicates that Ni/P alloys affect the dissolution rate of the passive film and improve the corrosion resistance. The results show that a stable and compact passive film was formed on the surface of the Cu–Ni/P composite coatings to ensure corrosion resistance.
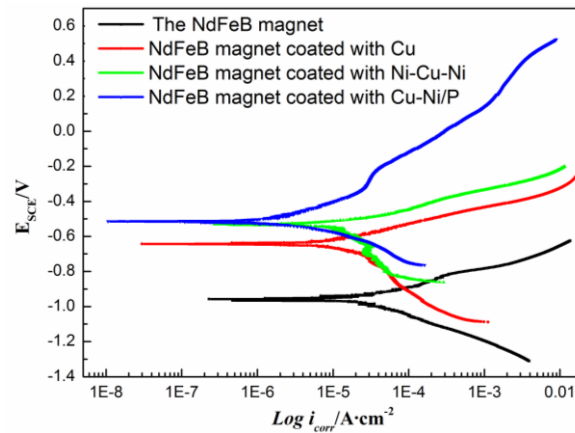
Figure 7. Potentiodynamic polarization curves of the NdFeB magnet, copper-coated NdFeB magnet, Ni–Cu–Ni coated NdFeB magnet and Cu–Ni/P composite coating immersed in 3.5 wt.% NaCl solution

Table 2. Corrosion potential (E_{corr}) and corrosion current density (I_{corr}) values

Specimens	E_{corr} (mV)	I_{corr} (Acm^{-2})
The uncoated	−960	3.4×10^{-4}
Cu coated	−676	2.6×10^{-4}
Ni–Cu–Ni coated	−532	2.5×10^{-4}
Cu–Ni/P coated	−515	1.6×10^{-6}

Table 2 shows that the E_{corr} value of the magnet coated with the Cu–Ni/P composite coating is higher than that of the magnet coated with the Ni–Cu–Ni coatings. Meanwhile, the I_{corr} value of the magnet coated with Cu–Ni/P composite coating is much lower than that of the magnet coated with Ni–Cu–Ni coatings, which reveals that Cu–Ni/P composite coatings have excellent anti-corrosion performance, because corrosive media coatings can generate a continuously dense, blunt film. No grain boundaries, dislocations, stacking faults, intergranular corrosion, or other defects were formed in crystalline metal, considering that amorphous Ni/P alloy has a disordered atomic arrangement. Amorphous Ni/P alloy also has good chemical and electrochemical uniformity and lacks corrosion nucleation centers and, therefore, is corrosion resistant..

EIS spectra of the specimens were obtained in neutral 3.5 wt.% NaCl solution. In Figs. 8 and 9, the Nyquist plots and Bode plots for the four specimens are displayed, respectively.
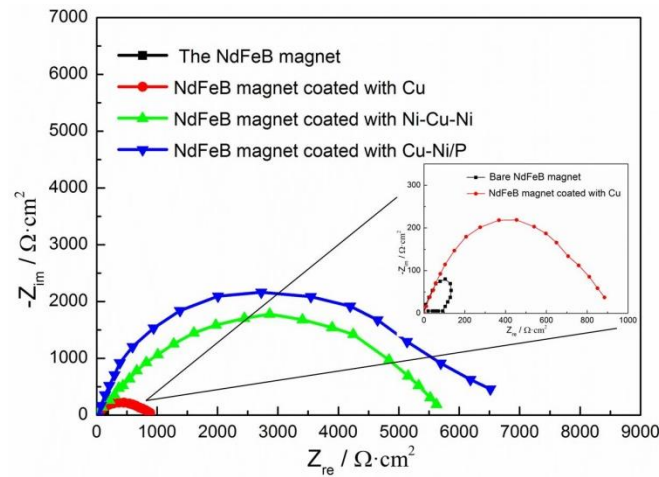
Figure 8. Nyquist plots of bare NdFeB magnet, copper-coated NdFeB magnet, Ni–Cu–Ni coated NdFeB magnet and Cu–Ni/P composite coating immersed in 3.5 wt.% NaCl solution
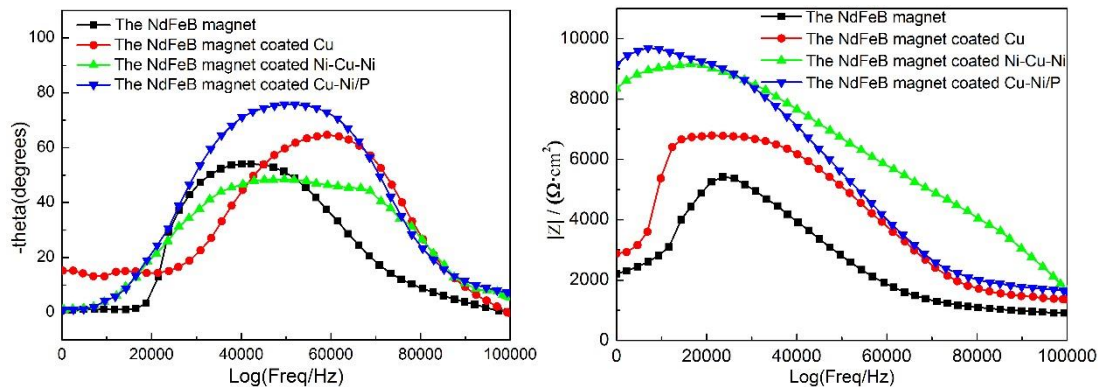
Figure 9. Bode plots of bare NdFeB magnet, copper-coated NdFeB magnet, Ni–Cu–Ni coated NdFeB magnet and Cu–Ni/P composite coating immersed in 3.5 wt.% NaCl solution

As shown in Fig. 8, in the Nyquist plot, the magnets coated with copper coating can be seen, Ni–Cu–Ni coatings and Cu–Ni/P composite coatings display similar shapes of single semicircles. The radii of the semicircle arcs are interrelated to the polarization resistance of the surface coating. The radii of the Ni–Cu–Ni coatings and Cu–Ni/P composite coatings are larger than the NdFeB magnetic material. For the Cu–Ni/P composite coating, the arc radius is slightly larger than the Ni–Cu–Ni coatings. This indicates that the magnet coated with the Cu–Ni/P composite coating exhibits better corrosion resistance.

As can be seen from the Bode plots, both copper-coated magnets and the Cu–Ni/P composite coated magnets exhibit a single time constant in Fig. 9. The electrochemical equivalent circuit as shown in Fig. 10(a) was used for bare NdFeB magnet, electrolyte solution resistance R_s, charge transfer resistance R_{ct1}, inductance resistance R_L, inductance L, and constant phase element (CPE_1) [34]. Fig. 10(b) shows the electrochemical equivalent circuit and parameters, where R_s stands for solution resistance, R_{ct1} for charge transfer resistance, and CPE_1 for a constant phase element. CPE_1 was used to

replace the capacitance of the electrical double layer (C_{dl}), because the electrode surface does not behave ideally owing to the distribution of currents and electroactive species [35]. *CPE* represents the constant phase angle element, and *Y* is a *CPE* device admittance; $Z_{CPE} = Y_0^{-1}(j\omega)^{-n}$, $0 < n < 1$, $0 < n < 1$. Therefore, the equivalent element of *CPE* has two constants: a parameter Y_0, units$\Omega^{-1}cm^{-2}s^{-n}$, and the diffusion coefficient n. When n = 1, the *CPE* is equivalent to a pure capacitance; when n = 0, the *CPE* is equivalent to a pure electric resistance; and when n = −1, the *CPE* is equivalent to an inductor. In general, the *CPE* behavior could be considered a "ω space fractality," i.e., as a manifestation of a self-similarity in the frequency domain [36]. The fitted values are summarized in Table 3 by the ZSimpWin. R_{ct1} values directly correspond to the corrosion resistance. The R_{ct1} value of the magnet coated with Cu–Ni/P composite coating is 6406 Ωcm^2, which is larger than that of the magnet coated with a Ni–Cu–Ni coating with an R_{ct} of 5468 Ωcm^2. R_{ct1} is a reflective coating on the surface of the base material of the protective effect of an intuitive argument. Given that coating impedance is inversely proportional to the corrosion current, greater resistance values of the coating in corrosive environments indicates better corrosion resistance.
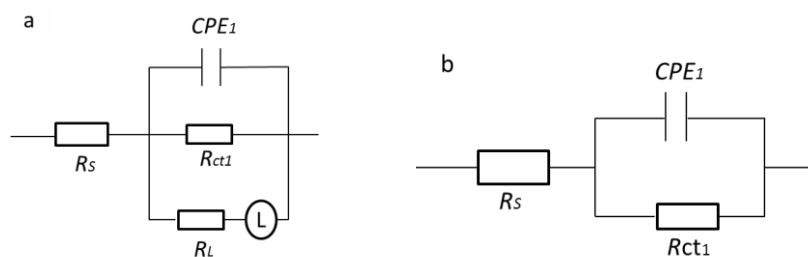
Figure 10. Electrochemical equivalent circuits used for fitting the experimental data of the bare NdFeB magnet (a), copper-coated NdFeB magnet, Ni–Cu–Ni coated NdFeB magnet and Cu–Ni/P composite coating (b). R_s: solution resistance. CPE_1: constant phase element. R_{ct1}: charge–transfer resistance. R_L: inductance resistance. L: inductance
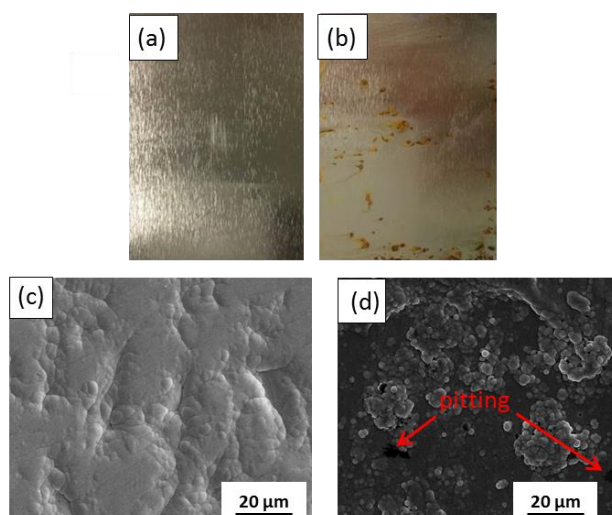
Figure 11. NSS tests of the Cu–Ni/P coated NdFeB(a), Ni–Cu–Ni coated NdFeB magnet(b), SEM images of the Cu–Ni/P coated NdFeB after NNS tests(c), SEM images of the Ni–Cu–Ni coated NdFeB after NNS tests(d)

Table 2. Electrochemical parameters fitted from EIS measurement impedance data of the NdFeB magnet, copper-coated NdFeB magnet, Ni–Cu–Ni coated NdFeB magnet and Cu–Ni/P composite coating immersed in 3.5 wt.% NaCl solution

Specimens	Rs (Ωcm^2)	$Y_0(\Omega^{-1}cm^{-2}s^{-n})$	n	$Rct1(\Omega cm^2)$	$R_L(\Omega cm^2)$	$L(\Omega cm^2)$
The uncoated	2.5	2.3×10^{-3}	0.7	250.1	56.1	99.2
Cu coated	3.5	1.2×10^{-4}	0.8	544.1		
Ni–Cu–Ni coated	4.1	7.8×10^{-5}	0.8	5468		
Cu–Ni/P coated	5.0	5.6×10^{-5}	0.89	6406		

The EIS results, which were confirmed by NSS tests, indicate that Cu–Ni/P coated NdFeB can stand for ~120 h in neutral 5.0 wt.% NaCl salt spray (35 °C) without pitting corrosion in Fig. 11(a) and (c). After NNS tested in 5.0 wt.% NaCl, the surface of the coating still shows metallic luster. However, the Ni–Cu–Ni coated NdFeB can stand for ~120 h in neutral 5.0 wt.% NaCl salt spray (35 °C), as shown in Fig. 11(b) and (d) , the corrosion morphology of the coating, Pitting corrosion occurred on the surface layer of Ni–Cu–Ni coated NdFeB. The corrosion of nickel is mainly due to the presence of chloride ions in 5.0 wt.% NaCl. The corrosion process of nickel is the depolarization process of oxygen and the corrosion rate is controlled by the diffusion process of oxygen. It is an inverse relationship between the resistance value and the corrosion current, and the test results are consistent with the measurement results of the polarization curves. Therefore, smaller corrosion current result in greater values of coating impedance. These results explain that the coating with Cu–Ni/P has better a corrosion resistance and protection characterization than copper coating for the magnets.

4. CONCLUSIONS

The obtained results enable the following conclusions to be drawn:

(1)　Plated Cu coatings were successfully produced on the NdFeB magnet and exhibited good binding force.

(2)　Corrosion analysis of the magnet coated with composite coating indicated that Cu–Ni/P composite coatings provided excellent anti-corrosion property for NdFeB magnet based on the I_{corr}, E_{corr}, and R_{ct} values.

(3)　Compared with the traditional plating of Ni–Cu–Ni multilayer coatings, the new Cu–Ni/P composite coatings, which were prepared using fewer steps, can achieve the better effect.

References

1. Y. Li, H.E. Evans, I.R. Harris, I.P. Jones, *Oxid. Met* . 59 (2003) 167.
2. J. Chen, B. Xu, G. Ling, *Mater Chem Phys*., 134 (2012) 1067.
3. A. Saliba-Silva, R .N. Faria , M.A. Baker, I. Costa, *Surf. Coat. Technol*. 185 (2004) 321.
4. Nan H, Zhu L, Liu H and Li, W: *Appl Surf Sci*. 355 (2015) 1215.
5. J. Zheng, H. Chen, L. Qiao, M. Lin, L. Jiang, S. Che, Y. Hu, *J Magn Magn Mater*., 371 (2014) 1.
6. M. Pan, P. Zhang, X. Li , H. Ge, Q. Wu, Z. Jiao, T. Liu, *J. Rare. Earth*., 28 (2010) 399.
7. R. Sueptitz, S. Sawatzki, M. Moore, M. Uhlemann, O. Gutfleisch, A. Gebert, *Materand Corros*., 66 (2013) 152.
8. A. Ali, A. Ahmad, K. M. Deen, *J. Rare. Earth*., 27 (2009) 1003.
9. W. Q. Liu, Z. Wang, C. Sun, M. Yue, Y. Q. Liu, D. T. Zhang, J. X. Zhang, *Appl Phys*., 115 (2014) 17A716.
10. D. J. Zhou, J. H. Wang, Y. Gao, L. Zhang, *Int. J. Electrochem Sci*., 12 (2017) 192.
11. H. Zhang, Y. W. Song, Z. L. Song, *Mater Corros.,* 59 (2008) 324.
12. E. H. A. Addi, I. Zaanoun, A. A. Addi, A. Found, L. Bazzi, A. Outzouighit, *Int. J. Electrochem.Sci*., 8 (2013) 7842.
13. Y. W. Song, H. Zhang, H. X. Yang, Z. L. Song, *Mater Corros*., 59 (2008) 794–801.
14. H. M. Luo, Y. F. Yang,Y. X. Sun, X. Zhao, J. Q. Zhang, *J. Solid State Electr*., 19 (2015) 1171.
15. D.J. Zhou , J.H. Wang, Y. Gao, L. Zhang, *Int. J. Electrochem Sci.,* 12 (2017) 192.
16. F. Liu, Q. Li, X. K. Yang, Y. Dai, F. S. Y Luo,. Wang, H. X. Zhang, *Mater Corros.,* 62 (2011) 1141.
17. J.H. Wang, L. Zhang, Y. Gao, X. Liu, W. B. Hu, *Int. J. Electrochem Sci*., 14 (2019) 59.
18. C.Y. Wan, L. Zhang, X.Y. Liu, *Int. J. Electrochem. Sci*., 15 (2020) 26.
19. Y. Hu, M. Aindow, I. Jones, I. Harris, *J. Alloy Compd*., 351 (2003) 299.
20. K. Majima, S. Sunada, H. Ito, Y. Kaneko, *J. Alloy Compd*., 408 (2006) 1426.
21. Z. Chen, A. Ng, J. Yi, X. Chen, *J. Magn Magn Mater*., 302 (2006) 216.
22. X. G. Cui, M. Yan, T. Y. Ma, L. Q. Yu, *Physica B.,* 403 (2008) 4182.
23. J. M. Hu, X. L. Liu, J. Q. Zhang, C. N. Cao, *Prog Org Coat*., 55 (2006) 388.
24. I. Rampin, F. Bisaglia, M. Dabalà: *J. Mater Eng Perform*., 19 (2009) 970.
25. V. R. Rao, H. A. Chitharanjan, *Prot Met Phys Chem+*., 49 (2013) 693.
26. A. Ali , A. Ahmad, *Mater Corros*., 60 (2009) 372.
27. X. M. Yu, Y.L. Huang, W.J. Qu, A.P. Yadav, R.D. Marco, *Int. J. Electrochem. Sci*., 9 (2014) 3760.
28. E. Valova, J. Georgieva, S. Armyanov, I. Avramova, J. Dille, O. Kubova, M. P. Delplancke-Ogletree, *Surf Coat Tech*., 204 (2010) 2775–2781.
29. J. Ni, X. Cui, X. Liu, H. Cui, Z. Xue, Z. Jia , S. Gong, *Mater Chem Phys*., 162 (2015) 518–524.
30. F. Fabiano, F. Celegato, A. Giordano, C. Borsellino, L. Bonaccorsi, L. Calabrese, B. Azzerboni, *Physica B.,* 435 (2014) 92.
31. Yuan. X, Sun. D, Yu. H, Meng. H, Fan. Z, & Wang. X, *Surf Coat Tech*., 202(2007), 294.
32. C. Ma, F. Cao, Z. Zhang, J. Zhang, *Appl Surf Sci*., 253(2006), 2251.
33. X. Dong, D. Wang, Y. Zeng, *J. Rare. Earth*., 32(2014), 867.
34. B. Szczygieł, M. Kołodziej, *Electrochim Acta*., 50 (2005) 4188.
35. J.M. Calderon-Moreno, C. Vasilescu, S. I. Drob, S. Ivanescu, P. Osiceanu, P. Drob, M. Popa, S. Preda, E. Vasilescu, *J. Alloy Compd*., 612 (2014) 398.
36. R. M. Elsherif, K. M. Ismail, W. A. Badawy, *Electrochim. Acta*, 49 (2004) 5139.